Electronic structure of ferric doped montmorillonite and its application to photocatalytic reduction of chromate

Li Zhang[1], Chitiphon Chuaicham[1], Keiko Sasaki[1]

[1]*Department of Earth Resources Engineering, Faculty of Engineering, Kyushu University, Fukuoka 819-0395, Japan*

Abstract

Clay based photocatalysts have been reported to be highly active photocatalysts for the environmental and energy applications because of unique 2D structures and optical properties. In this work, Fe(III)-modified montmorillonite was prepared by ion-exchange for the photocatalytic reduction of toxic $Cr(VI)_2O_7^{2-}$. The best performance was observed with the Fe(III) modified montmorillonite with 0.377 mmol-Fe(III)/g. The enhancement of photocatalytic activity of Fe(III)-modified montmorillonite might be derived from not only the reduction of energy band gap but also the generation of new electronic levels from Fe(III) between the valence band and the conduction band of montmorillonite. The new electronic state from Fe(III) could accept the electrons from valence band of montmorillonite to avoid the recombination of the electron-hole pairs. Moreover, the reusability of Fe(III)-modified montmorillonite was evaluated. The photocatalytic activity decreased after the repeated cycles, which is due to the releasing of Fe(III) from the modified montmorillonite. The finding can be used to develop a various clay based photocatalysts for wastewater treatment and beyond.

1. Introduction

Montmorillonite (Mt) is a representative 2:1-type of clay mineral with one octahedral Al–O(H) sheet sandwiched between two tetrahedral Si–O sheets in one layer. It has a high cation exchange capacity (~1.14 meq/g). The clay minerals have been often applied as supporting materials to make a better dispersion of the main material on them and improve the separation efficiency of the material from the liquid, for example environmental remediation materials [1], [2].

Although clay minerals were generally regarded to have no photocatalytic property [3], acid activated Mt endued the photocatalytic activities by generating the Brønsted acid sites [4]. So it has been found that the acid activated Mt can be utilized as a component of photocatalyst composites. However, the treatment of clay minerals requires very strongly acidic conditions, where the concentration of proton is usually > 5 M, and long time, usually for longer than 2 h [3], [4].

Iron (Fe) is one of widely distributed elements in the natural environments. The role of iron in the photocatalytic reaction arouses the researches interest. It seems like the Mt not only acts as a support material in the composite with the main photocatalyst, the clay minerals itself with iron doping can act as a photocatalyst independently. A Zn/Fe-layer double hydroxide (LDH) has been observed to photodegrade various azo dyes more efficiently than bare Fe_2O_3 or ZnO under visible light [5]. The authors proposed that this may be due to the important role that the Fe(III) ions in the FeO_6 octahedrons of the Zn/Fe LDH structure have in the absorbance of visible light. Also, the hydroxyl groups in the LDH capture the photo-induced holes (h^+) thus preventing the recombination of the h^+ and electron(e^-) leading to enhanced photoactivity [5]. Other researchers have attributed the prevention of recombination to the oxo-bridges between the two different metals in the brucite layer [6]. However, these assumptions explaining the mechanisms of Cr(VI) photocatalytic reduction are still controversial in the literature.

Up to our best knowledge, iron doped Mt has not been used for the photocatalytic reduction of Cr(VI). In the present work, Fe(III)-doped Mt with varied stoichiometry of Fe(III) dosage was synthesized at pH 2 within 1 h to use this for Cr(VI) photocatalytic reduction under acidic condition avoiding the precipitation of Fe(III) source, and elucidate the role of Fe(III) in the photocatalytic mechanisms of Cr(VI) reduction.

2. Materials and methods

2.1. Preparation of Fe(III)-modified Mt

Na-montmorillonite (Kunipia-F) was obtained from Kunimine Industries Co. Ltd. (Tokyo, Japan). To synthesize the Fe-Mts, Mt was dispersed into the solution where Fe(III) stoichiometrically equivalent to the 0.25, 0.5, 1, 2, and 4 times of CEC for Mt. Then Fe-Mts were collected and named depending on the added Fe(III). The remaining concentration of Fe(III) in supernatant was determined by an inductively coupled plasma-optical emission spectroscopy (ICP-OES; Perkin Elmer 8500, Waltham, MA, USA) and listed in **Table 1**.

2.2. Solid characterization

Powder X-ray diffraction (XRD) patterns of the original Mt and Fe-Mts were recorded using an Ultima IV X-ray diffractometer (Rigaku, Akishima, Japan). X-ray photoelectron spectroscopy (XPS) was conducted on an ESCA 5800 system (Ulvac-PHI, Kanagawa, Japan. The N_2- adsorption / desorption isotherms were measured on a BELSORP-max instrument (BEL Inc., Osaka, Japan). Diffuse reflectance spectra (DRS) were measured on a UV-2450 spectrophotometer (Shimadzu Co. Ltd., Kyoto, Japan). Scanning electron microscopy (SEM) images were observed using a VE-9800 SEM (Keyence, Osaka, Japan).

2.3. Photocatalytic activity test

The photocatalytic reduction of Cr(VI) were tested under a 300 W Xe lamp irradiation in 10 mg/L Cr(VI) solution with S/L=1:1 at pH 2.0 in a photoreactor with a cooling water jacket outside. After the adsorption/desorption equilibrium within 10 min, ~ 1 mL of the suspensions was sampled from the reaction cell at appropriate. The remaining Cr(VI) was determined by the carbazide method with a UV–Vis spectrophotometer (UV-2450, Shimadzu, Kyoto, Japan) at 540 nm.

3. Results and discussion

3.1. Characterizations

The 001 reflection in XRD of the original Mt emerged at 7.25° in 2θ is correspondent to the interlayer distance to be 1.21 nm including the thickness of one Mt layer (0.96 nm). Even without any Fe(III) addition, the H-Mt still shows correspondingly to the similar interlayer distance (~1.39 nm) with other Fe-Mt. The expanded interlayer space in H-Mt is attributed to the migration of the structural Fe(II)/Fe(III) from the aluminosilicate layers to the interlayer. As for other Fe-Mt, the expansion of interlayer distance was dominated by both the intercalation of Fe(III) and the migration of the structural iron.

In the preparation of Fe-Mt, the immersion of the Mt into The Fe(III) solution at low pH generated some defects on the Mt structure, which confirmed by the release of Fe in H-Mt. Not only the added Fe(III) from Fe(III) solution can intercalate into the interlayer space of Mt, but also the Fe(III) baring in the original Mt structure can diffuse/migrate to the channel of Mt layers. The dynamic of the structural iron and added Fe(III) in the interlayer space was not detectable, but the dynamics of iron species in the solution was detected by ICP-OES and listed in **Table 1**. With the increase of the initial Fe(III) addition, the doped amount of Fe(III) increased in H-Mt, 0.25Fe-Mt, 0.5Fe-Mt, and 1Fe-Mt; and tended to be stable when it was over 1 time CEC of Mt. Based on the chemical formula of the Kunipia F, the Na(I) engages ~0.858 meq/g charges on Mt layers. As the adsorbed Fe(III) reached a sub-saturated state of 0.720 meq/g in 1Fe-Mt, most of the Na(I) sites were replaced by Fe(III). The additional Fe(III) intercalated should start to occupy the Ca(II) exchangeable sites which require more change in entropy.

Table 1 Fe(III) loading amount, d_{001}-value of Mt, S_{BET}, and E_g of Fe(III) modified Mts

Sample	adsorbed Fe(III) [1]		d_{001} [2]	E_g [3]
	Q (mmol/g)	meq/g	(nm)	(eV)
H-Mt	-0.001	-0.003	1.38	3.50
0.25Fe-Mt	0.091	0.238	1.38	3.10
0.5Fe-Mt	0.175	0.462	1.38	2.70
1Fe-Mt	0.274	0.720	1.38	2.65
2Fe-Mt	0.299	0.786	1.38	2.60
4Fe-Mt	0.312	0.822	1.40	2.60

[1] Calculated based on ICP-OES measurement.

[2] Estimated by XRD.

[3] Evaluated by Tauc plotting Kubelka–Munk function versus the energy.

The SEM images for the H-Mt were similar to the original Mt (**Fig. 1**). As the addition of Fe(III) increased, the stacked layers tend to be non-parallel lead to the increase of face to edge cross and the Mt layers on the surface broke down into smaller layers. From the N_2 adsorption/desorption isotherm, the type IV curve implied the mesoporous features of samples.

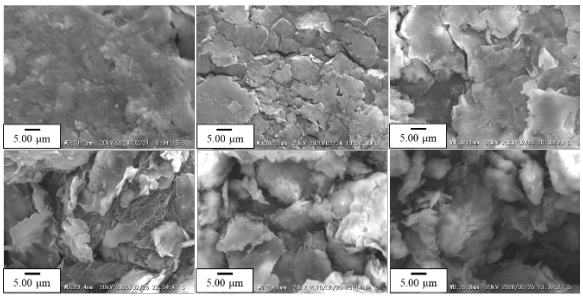

Fig. 1 SEM images of (a) H-Mt, (b) 0.25Fe-Mt, (c) 0.5Fe-Mt, (d) 1Fe-Mt, (e) 2Fe-Mt and (f) 4Fe-Mt.

3.2. Optical and charge separation properties

The UV–vis diffuse reflectance spectra (UV-DRS) of Fe-Mt showed a significant red shift of the absorption edge as compared to H-Mt (**Fig. 2**) which significantly improved the optical property of the samples. The band gap energy (E_g) of Fe-Mt can be evaluated according to Eq. (1):

$$\alpha hv = k(hv - Eg)^{n/2} \quad (1)$$

where α, h, v, k, and Eg represents the absorption coefficient, Planck constant, light frequency, band gap energy, and the proportionality constant, respectively.

The value of n is dependent on the type of optical transition of the measured semiconductor (direct transition at $n = 1$ and indirect transition at $n = 4$). The calculated band gap values of the samples were estimated to be approximately 3.50, 3.10, 2.70, 2.40, 2.40, and 2.38 eV for H-Mt, 0.25Fe-Mt, 0.5Fe-Mt, 1Fe-Mt, 2Fe-Mt, and 4Fe-Mt (**Table 1**). The XPS revealed the valence band (VB) energy was around 2.0 eV. Therefore, the conduction band energy (CB) of 1Fe-Mt is −0.65 eV.

The correlated Fe(III)-doping (**Table 1**) and the Eg from H-Mt to 1Fe-Mt enhanced the photo-generation of charge carriers (e^- and h^+) which may was caused by the formation of new middle gap level(s) driven from the doped Fe(III). Additional Fe(III) trapped the e^- from the Cr(VI) or overlapped to compete converting the light.

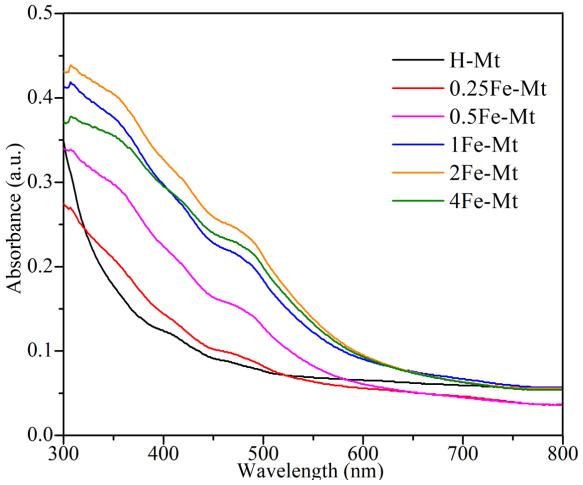

Fig. 2 DRS-UV spectra of Fe-Mt.

3.3. Photocatalytic activity

Fig. 3 shows the Cr(VI) removal in the presence of Fe-Mts. Under the dark condition, slight adsorption of Cr(VI) with ~2- 6% was observed. Bichromate ($Cr_2O_7^{2-}$) is unlikely to be adsorbed on Mt in itself, but the adsorbed Fe(III) might be electrostatically bound with it. Under light irradiation, the H-Mt showed only around 20% reduction of Cr(VI) after 60 min. As is suggested in XRD result (**Table 1**), Fe(III)/Fe(II) in the octahedral sheet diffused to the interlayer which has an improved effect on the optical property and photocatalytic activity of H-Mt. With further Fe(III) loading in 0.25Fe-Mt and 0.5Fe-Mt, the improvement of Cr(VI) reduction was related to the enhanced effect of newly added interlayer Fe(III) and the removal of Cr(VI) reached 22% and 35%. When the interlayer doped Fe(III) amount increased to 0.274 mmol/g-Mt in 1Fe-Mt, the photocatalytic reduction of Cr(VI) reached to the maximum with 47%. A slight increase of Fe(III) loading in 2Fe-Mt and 4Fe-Mt slightly reduced the performance, with 44% and 43% efficiency. The kinetics of Cr(VI) photocatalytic reduction fitted to the pseudo-first-order kinetics (Eq. 2):

$$-\ln(C/C_0) = kt \quad (2)$$

where C and C_0 (mmol/g) are the remaining and initial concentrations of Cr(VI), the k (min^{-1}) is the rate constants of the pseudo-first order model. The k are 2.97×10^{-3}, 5.30×10^{-3}, 6.31×10^{-3}, 10.52×10^{-3}, 9.22×10^{-3}, and 9.08×10^{-3} min^{-1}.

The inconspicuous difference of the surface morphology (**Fig. 1**) depending on doped amounts Fe(III) on Mt indicated to have a negligible effect on the photocatalytic reaction.

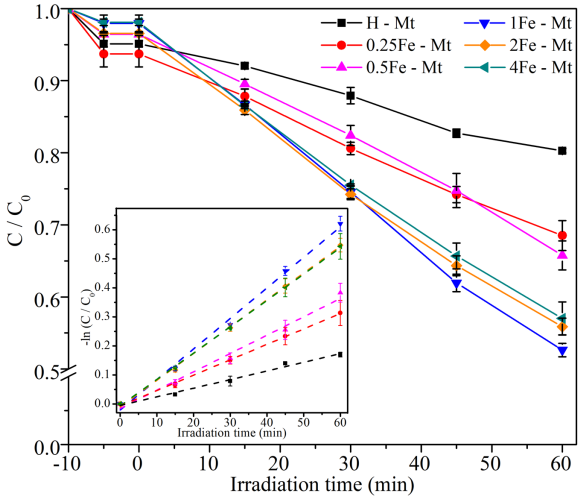

Fig. 3 Adsorption and photocatalytic reduction of Cr(VI) over Fe-Mt under irradiation time at pH 2, and (inset) the pseudo-first-order kinetic plot.

3.4. Mechanism of Cr(VI) reduction

The photocatalytic activity of Fe-Mt photocatalyst for Cr(VI) reduction can be described by the production of the e^--h^+ pairs induced through the transition of e^- under UV light [7]. The Fe-Mts showed significant increase in photocatalytic reduction of Cr(VI) compared with H-Mt. Also from the DRS and Eg (**Fig. 2**), the H-Mt sample showed larger Eg than Fe-Mts, indicating that the presence of iron in the structure of Mt might can reduce Eg of Mt by formation of new electronic level between VB and CB of Mt. Photo-generated charge carriers (e^- and h^+) of Fe-Mt were generated and separated at different electronic states: the photo-generated e^- can move to new middle gap state, and leaving photo-generated h^+ in the VB. For photocatalytic reduction of Cr(VI), the dissolved Cr(VI) in the solution could be reacted with an e^- in middle gap states and reduced it to Cr(III), while the h^+ remained in the VB or reacted with H_2O molecules to enhance the photocatalytic performance in Cr(VI) reduction. Reduced Cr(III) species should be partially adsorbed on the surface of Mt and deceasing its release into the solutions.

4. Conclusions

Fe(III)-doping significantly improved the photocatalytic reduction of Cr(VI) by Mt. The optimal doping amount of Fe(III) was 0.720 meq-Fe(III)/g-Mt showing 47% reduction of Cr(VI) while it was only 20% without doping Fe(III). However, the excess doping amounts of Fe(III) decreased the Cr(VI) photocatalytic reduction, probably because the extra of Fe(III) in the Fe-Mt can not only act as recombination center of e^-, leading to inhibition of e^- transfer in the Cr(VI) reduction, but also some Fe(III) cover on the surface of Mt, resulting to decrease in surface areas of Mt to receive the light. The Fe(III) might decide the generation of a new electronic level.

Acknowledgements

This work was supported by Kyushu University Progress 100 Strategic Partnership Acceleration, and Cooperative Research Programs at Hokkaido University Institute for Catalysis (Nos. 19B1002 and 20A1001), which were provided to KS. LZ sincerely appreciates the Advanced Graduate Program in Global Strategy for Green Asia.

References

[1] Z. Sun, C. Li, X. Du, S. Zheng, and G. Wang, "Facile synthesis of two clay minerals supported graphitic carbon nitride composites as highly efficient visible-light-driven photocatalysts," *J. Colloid Interface Sci.*, vol. 511, pp. 268–276, 2018.

[2] B. Szczepanik, "Photocatalytic degradation of organic contaminants over clay-TiO2 nanocomposites: A review," *Applied Clay Science*, vol. 141. Elsevier Ltd, pp. 227–239, Jun. 01, 2017.

[3] D. Chen, Q. Zhu, F. Zhou, X. Deng, and F. Li, "Synthesis and photocatalytic performances of the TiO2 pillared montmorillonite," *J. Hazard. Mater.*, vol. 235–236, pp. 186–193, Oct. 2012.

[4] F. Bergaya and G. Lagaly, *Handbook of clay science*. Newnes, 2013.

[5] K. M. Parida and L. Mohapatra, "Carbonate intercalated Zn/Fe layered double hydroxide: A novel photocatalyst for the enhanced photo degradation of azo dyes," *Chem. Eng. J.*, vol. 179, pp. 131–139, Jan. 2012.

[6] S. J. Kim, Y. Lee, D. K. Lee, J. W. Lee, and J. K. Kang, "Efficient Co-Fe layered double hydroxide photocatalysts for water oxidation under visible light," *J. Mater. Chem. A*, vol. 2, no. 12, pp. 4136–4139, Mar. 2014.

[7] W. N. Zhao, S. C. Zhu, Y. F. Li, and Z. P. Liu, "Three-phase junction for modulating electron-hole migration in anatase-rutile photocatalysts," *Chem. Sci.*, vol. 6, no. 6, pp. 3483–3494, Jun. 2015.

Email: zhang@mine.kyushu-u.ac.jp